MDPI

Article

Real-Time Monitoring of Laser Cleaning for Hot-Rolled Stainless Steel by Laser-Induced Breakdown Spectroscopy

Xing Li [1,2] and Yingchun Guan [1,2,3,*]

1   Hefei Innovation Research Institute, Beihang University, Hefei 230012, China; lixing1990@buaa.edu.cn
2   School of Mechanical Engineering and Automation, Beihang University, Beijing 100083, China
3   National Engineering Laboratory of Additive Manufacturing for Large Metallic Components, Beihang University, Beijing 100083, China
*   Correspondence: guanyingchun@buaa.edu.cn

Abstract: Laser cleaning is a competitive alternative to ablate and remove the hard oxide layer on hot-rolled stainless steel. To meet the practical demand, laser-induced breakdown spectroscopy (LIBS) was applied for real-time monitoring of the cleaning process in this study. Furthermore, the as-received and laser cleaned surfaces were characterized by an optical micrograph, an X-ray diffractometer, and a laser scanning confocal microscope. The results showed the relative intensity ratio (RIR) of the Fe_I emission line at 520.9 nm and the Cr_I emission line at 589.2 could be a quantitative index to monitor the cleaning process. When the oxide layer was not fully cleaned, the LIBS signals of the substrate were not excited, and the ratio was almost invariant as the power of the laser increased. However, it sharply increased once the oxide layer was effectively cleaned, the cleaned surface was bright, and the surface roughness was smaller in this case. Subsequently, as the surface was over-cleaned with the further increase of laser power, the RIR value remained large. The optimal laser cleaning parameters obtained by the monitoring were determined to avoid re-oxidation and reduce the roughness of the cleaned surface.

Keywords: laser cleaning; oxide layer; laser-induced breakdown spectroscopy; surface roughness

1. Introduction

Stainless steel has been widely used in the fields of construction, biomedical, and vessel building [1]. In the manufacturing process, the stainless steel is commonly subjected to melting, casting, and rolling, and an oxide layer is easily induced at elevated temperatures. The oxide layer not only has an adverse effect on the surface appearance and welding property but also may lead to steel plate sticking to a roller in the subsequent cold rolling process [2]. Therefore, the oxide layer on the surface needs to be cleaned before use or further processing of the hot-rolled steel. However, compared to low-alloy steel, the oxide layer on the stainless steel is so tightly connected with the substrate that only mechanical shot peening or strong acid pickling can be applied to remove it in the industry [3,4]. In this process, the efficiency of cleaning is low and the degree of environmental pollution is also great.

Laser cleaning has been considered as a high-efficiency and environmental-friendly cleaning technology [5], which is a promising method to remove contaminants including oil [6–8], paint [9,10], and oxide layers [11–13]. Mateo et al. [6] used the laser cleaning method to ablate oil spills on rocks and tools, and the non-direct contact cleaning method effectively suppressed surface damage. Furthermore, the underlying mechanism of paint removal was investigated by Han et al. [10]. The results showed that the thermal effect was the most favorable for the laser cleaning of pain, and the vaporization and laser-plasma effects should be avoided to improve the quality of the cleaned surface. Li et al. [13] used in-situ laser cleaning instead of degreasing and sand-blasting stages before thermal spraying on a Ti alloy. The interfacial physical contact was enhanced for the cleaning of

surface pollutants and oxide layer. The hot-rolled AA7024 aluminum alloy was cleaned by a nanosecond laser, and the cleaned surface was bright, and no surficial defect was induced. Additionally, the corrosion resistance of the alloy in 3.5 wt.% NaCl solution was increased after laser cleaning [14].

Notably, the oxide layer that needs to be cleaned is commonly non-uniform in practice; thus, real-time parameter optimization of the laser is urgently required to achieve effective cleaning under complex conditions. Some real-time diagnostic methods, including photoacoustic and optical monitoring, have been demonstrated [15]. A low-noise photoacoustic (PA) wave in the MHz range was introduced to monitor the over-layer ablation, effective cleaning, and damaged substrate stages during laser cleaning of stone [16]. When the fluence of the laser was increased, the numerical range of pulses required to effectively clean the black graffiti became small. Similarly, Xie et al. [17] integrated the acoustic emission and a high-speed camera to monitor laser de-rusting, showing that the significant acoustic emission in the targeted frequency range could reveal the degree of laser cleaning. In the study of Senesi et al. [18], laser-induced breakdown spectroscopy (LIBS) was coupled to the laser cleaning of black crusts on limestone. The elemental composition of the crust and underlying stone were determined by the plasma spectral analysis. Then, the experimental conditions could be optimized in real-time to completely ablate the black crust without damaging the substrate. Marimuthu et al. [19] implemented a LIBS system into a laser cleaning cell, and the cleaning process of a TiAlN coating on the WC cutting tool was monitored. As the coating was cleaned, the peaks for Ti emission disappeared. By using a closed-loop cleaning system, a coating with variable thickness could be cleaned without artificial optimization of the laser parameters. However, little attention was paid to the online monitoring of oxide layer removal during laser cleaning of stainless steel.

In this study, laser cleaning was adopted to remove the oxide layer on the hot-rolled stainless steel. LIBS, which allows the fast elemental characterization on the surface of the material without sample preparation [20–22], was used to monitor the cleaning process online. The phase composition and morphology of the as-received and laser cleaned surfaces were characterized to illustrate the surface cleaning quality. The aim was to provide a way for the real-time optimization of parameters during laser cleaning of the oxide layer on hot-rolled stainless steel and promote the application of laser cleaning in this field.

2. Materials and Methods

2.1. Sample Preparation

A commercial hot-rolled 444 type ferritic stainless steel was selected for the study, and the thickness of the plate was 4 mm. Steel is a widely used commercial material. According to the national standard of China (GB/T 12770-2012), the chemical compositions in the weight percentage of the steel are shown in Table 1. The laser cleaning process was conducted on a 50 mm by 50 mm flat plate machined from the hot-rolled plate.
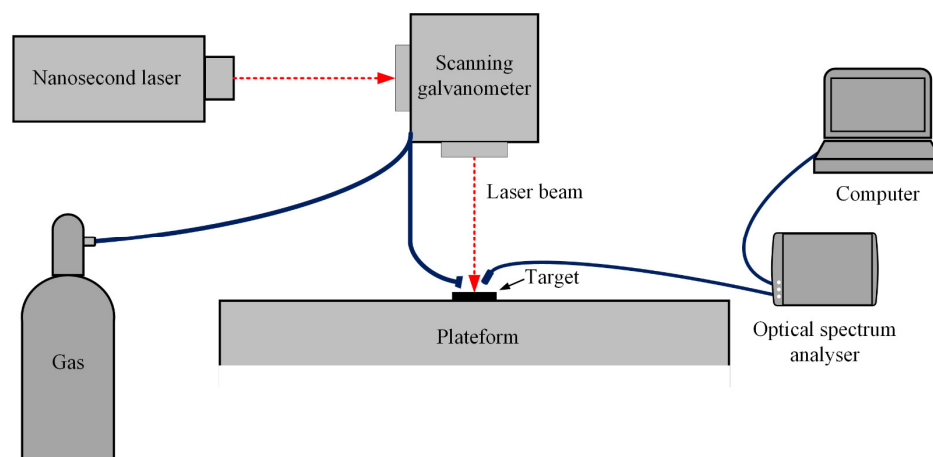
Table 1. Chemical compositions of the commercial hot-rolled 444-type stainless steel.

Elements	C	Cr	Mo	Ni	Si	Mn	N	P	S	Ti + Nb	Fe
Content (wt.%)	≤0.025	17.5–19.5	1.75–2.5	≤1.00	≤1.00	≤1.00	≤0.035	≤0.04	≤0.03	≥0.2 + 4 (%C + %N)	Bal.

2.2. Laser Processing and Real-Time Monitoring

As shown in Figure 1, laser cleaning of the hot-rolled steel was conducted using a nanosecond laser processing system with galvanometric scanning, and an SPI nanosecond laser (power = 70 W, wavelength = 1064 nm, pulse duration = 24 ns, repetition rate = 55 kHz, spot size = 30 μm) was used. The laser cleaning process was conducted under various laser powers, ranging from 20% to 90% of maximum power (denoted by $P_{20\%}$–$P_{90\%}$). The scanning speed remained at 500 mm/s, with one at the scanning time. The surface of the

sample to be cleaned was placed at the focus position of the laser, and the cleaned region was a 4 mm × 4 mm square using a hatched scanning mode with 50% overlap. Through a side nozzle with a flow rate of 5 L/min, Argon (Ar) was used as the protection gas. The optical signals induced during the laser cleaning were monitored by an optical spectrum analyzer (OSA, FLX 2000L, Fuxiang Optics, Shanghai, China). The background noise was deduced directly after the optical spectrums were obtained. The typical strong peaks of spectra were compared with NIST's Atomic Spectra Database (Version 5.7, American) for identification.

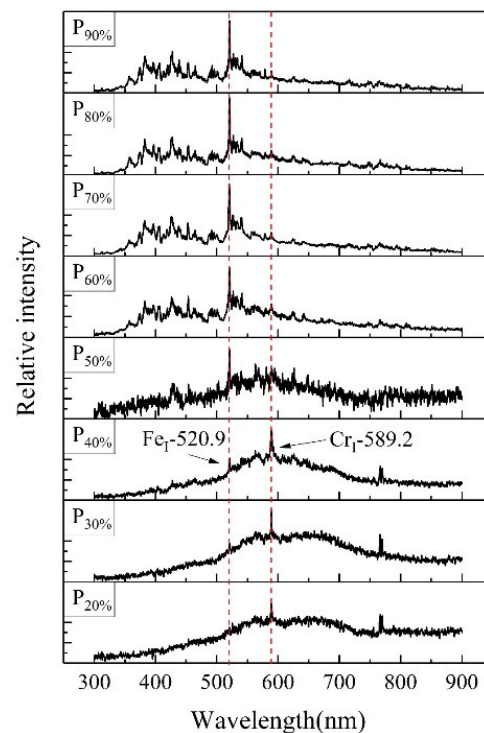**Figure 1.** Schematic diagram of the laser cleaning system.

2.3. Characterization

After laser cleaning, the typically cleaned surfaces were further studied to determine the cleaning effect. An optical micrograph (OM, Olympus BX53M, Olympus, Tokyo, Japan), an X-ray diffractometer (XRD, Smart Lab, Cu Kα, Rigaku, Tokyo, Japan), and a laser scanning confocal microscope (LSCM, Keyence VK-X, Keyence, Osaka, Japan) were used to characterize the results of laser cleaning. By using the three-dimensional surface profilometer obtained by LSCM, the average surface roughness Ra at three parallel lines was calculated by software directly. The direction of the lines was vertical to the laser beam travel direction. The samples for the OM analysis were mechanical polished and then etched in a solution of 5 g $FeCl_3$ + 50 mL HCl + 150 mL H_2O. The scanning range of XRD analysis was 40–100°, and the scanning speed was 5°/min. Based on the results of the LSCM analysis, the surface roughnesses of the as-received and laser-cleaned surfaces were calculated.

3. Results
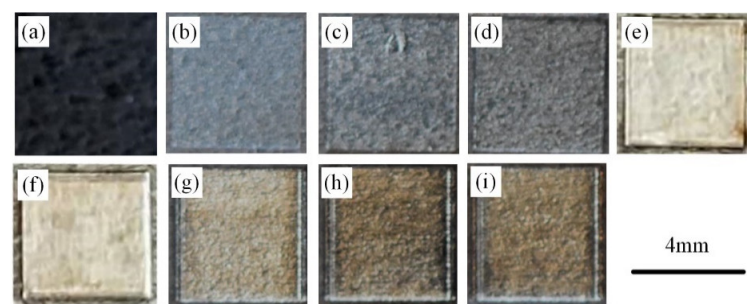
3.1. Optical Spectra during Laser Cleaning

Figure 2 shows the optical spectra obtained during the laser cleaning at varied laser powers. As the spectral intensity was also closely related to several factors, such as the distance between the probe and laser processing position, the relative intensity was used to analyze the behavior of the signal variation. When the laser power was low, the number of excited LIBS peaks was low, and the strongest peak was Cr_I-589.2. At $P_{50\%}$, the relative intensity of line Fe_I-520.9 increased significantly and became the strongest one, while the relative intensity of line Cr_I-589.2 decreased. In addition, abundant lines were also excited in the wavelength range 300–500 nm when the power of the laser increased.

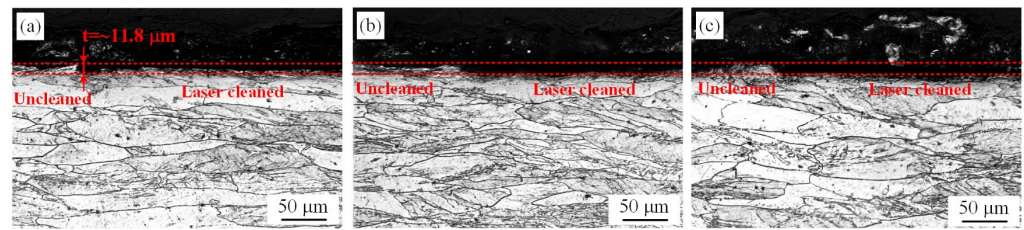**Figure 2.** Optical spectra obtained during the laser cleaning of the oxide layer at varied laser powers.

3.2. Characterization of the Laser Cleaning Surface

The macroscopic morphologies of the as-received and laser-cleaned surfaces are shown in Figure 3. When the power of the laser was lower than 28 W ($P_{40\%}$), the color of the oxide layer was close to that of the as-received surface (black), which indicated the oxide layer was not fully cleaned in these cases. At $P_{50\%}$ and $P_{60\%}$, the cleaned surfaces were bright, which was the desired result of cleaning. However, the color of the cleaned surfaces started to become brown when the laser power was increased to 49 W ($P_{70\%}$); the stainless steel was over-cleaned and experienced a large thermal effect.
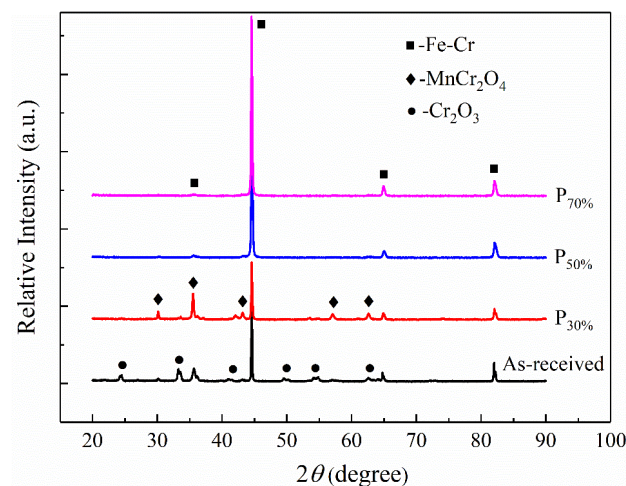

Figure 3. Macroscopic morphologies of the as-received (**a**) and laser cleaned surfaces at (**b**) $P_{20\%}$, (**c**) $P_{30\%}$, (**d**) $P_{40\%}$, (**e**) $P_{50\%}$, (**f**) $P_{60\%}$, (**g**) $P_{70\%}$, (**h**) $P_{80\%}$, and (**i**) $P_{90\%}$.

To further characterize the cleaning results, the cross-section morphologies of typical laser cleaned surfaces ($P_{30\%}$, $P_{50\%}$, and $P_{70\%}$) were studied, as shown in Figure 4. After hot rolling, the microstructure of the steel was an elongated ferrite, the oxide layer was inhomogeneous, and its thickness was ~11.8 μm. As shown in Figure 4a, the ablation of material was not obvious at $P_{30\%}$ for the low laser fluence. At $P_{50\%}$, the oxide layer was effectively cleaned (Figure 4b). When the power was further increased to 49 W ($P_{70\%}$), the thickness of the material ablated was also equal to that of the oxide layer (Figure 4c); it did not vary noticeably compared with $P_{50\%}$.

Figure 4. Optical micrograph (OM) images of the cross-section of hot-rolled stainless steel after laser cleaning at (**a**) P$_{30\%}$, (**b**) P$_{50\%}$, and (**c**) P$_{70\%}$.
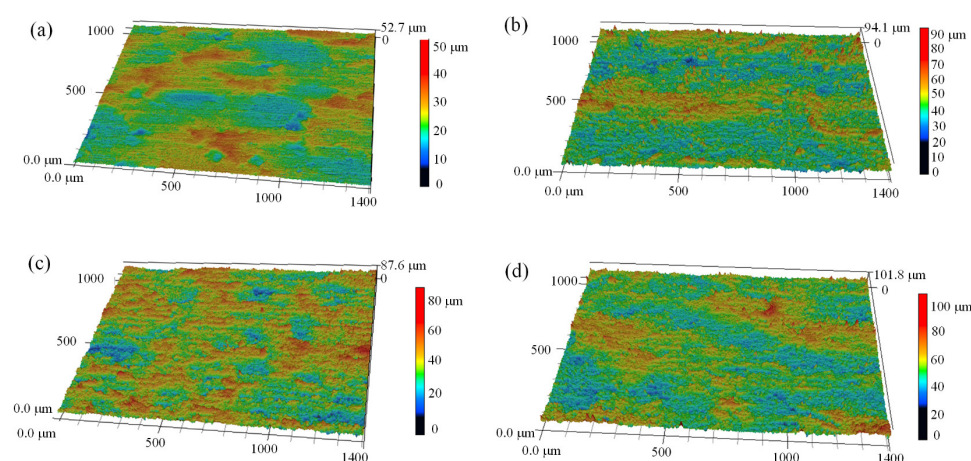
XRD patterns in Figure 5 illustrate the surface phase composition of the stainless steel before and after laser cleaning. Combining the characterization results of previous studies [23,24], the oxide products were determined as $MnCr_2O_4$ and Cr_2O_3. When the laser cleaning was conducted at P$_{30\%}$, most peaks of oxidation remained because the oxide layer was not fully cleaned. As the power of the laser was increased to 35 W (P$_{50\%}$) or 49 W (P$_{70\%}$), only the substrate Fe-Cr could be detected, showing that the previous oxide layer was cleaned in these two cases. The phase induced by re-oxidation during laser cleaning at P$_{70\%}$ was not detected because the oxidation products were too low under the shield of Ar.

Figure 5. X-ray diffractometer (XRD) patterns of the surface before and after laser cleaning at typical powers.

As shown in Figure 6, the morphologies of the as-received and laser cleaned surfaces were analyzed by LSCM, and the surface roughness (Ra) of the test area was directly calculated by the software. As shown in Figure 6a, the oxide scales on the surface were elongated by the hot rolling process. Since some oxide scales were broken during previous processing and then re-oxidation occurred during the following hot working, some massive depressions can be observed on the surface. In addition, some small hollows formed on the as-received surface because the broken oxide scales on the surface plate and roller were impressed during the hot rolling. As the surface was laser-cleaned, some grooves were induced by the laser scanning (Figure 6b–d). As shown in Table 2, the surface roughness increased from 3.8 to 5.8 μm after laser cleaning at P$_{30\%}$. At P$_{50\%}$, where the oxide layer was effectively cleaned, the surface roughness was decreased to 5.5 μm. However, the surface roughness increased to 6.3 μm when the surface was over-cleaned at P$_{70\%}$.

Figure 6. Laser scanning confocal microscope (LSCM) images showing the 3D morphology of (**a**) as-received and laser-cleaned surfaces at (**b**) $P_{30\%}$, (**c**) $P_{50\%}$, and (**d**) $P_{70\%}$.
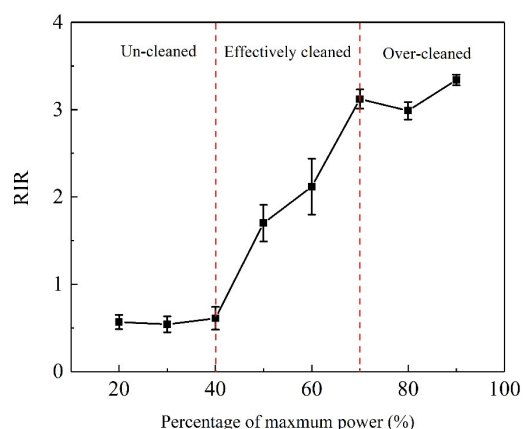
Table 2. Surface roughness of as-received and laser-cleaned surfaces.

Process	As-Received	$P_{30\%}$	$P_{50\%}$	$P_{70\%}$
Surface roughness Ra (μm)	3.8 ± 0.48	5.8 ± 0.36	5.5 ± 0.53	6.3 ± 0.32

4. Discussion

4.1. The Analysis of the LIBS Monitoring Process during Laser Cleaning

According to the optical spectral lines monitored during laser cleaning and the characterization of the cleaned surfaces, the strong peaks of Fe_I-520.9 and Cr_I-589.2 were closely related to the results of the laser cleaning. Thus, the relative intensity ratio (RIR) of Fe_I-520.9 and Cr_I-589.2 was used to qualitatively evaluate the cleaning process. As shown in Figure 7, when the oxide layer on the hot-rolled stainless steel was not fully cleaned, the laser beam only interacted with the oxide layer during laser cleaning the RIR was substantially retained because the main constituent phases of the oxide layer were $MnCr_2O_4$ and Cr_2O_3. At $P_{50\%}$, the oxide layer was effectively cleaned, the laser beam interacted with the substrate, and the RIR sharply increased because the relative intensity of Fe_I-520.9 increased significantly. When the surface was over-cleaned at a large laser power, all LIBS signals of the substrate and oxide layers were excited during the laser irradiation; the RIR began to level off. However, the thermal effect was too large when the power of the laser was increased, re-oxidation occurred during laser cleaning even though Ar was used as a shielding gas. Consequently, the color of the cleaned surface became brown.

Figure 7. The variation of relative intensity ratio (RIR) with the power of laser during laser cleaning of the oxide layer.

Hence, the RIR obtained by online LIBS monitoring could be used as an index for real-time adjustment of the cleaning parameters during the laser cleaning of the oxide layer on hot-rolled stainless steel. In a practical process, the preliminary parameters of the laser could be determined by experimental research. To reduce the energy cost and avoid over-cleaning, it was suggested to reduce the power of the laser as much as possible during laser cleaning, as long as the RIR did not become too low. As the cleaning threshold of the oxide layer was increased, for reasons such as local thickening, the RIR would significantly decrease, and then the power of the laser should be dynamically increased, based on the online LIBS monitoring. Owing to the advantages of high flexibility and environmental protection, the laser cleaning with real-time monitoring had the potential to be used to ablate the oxide layers on the hot-rolled steel. To further promote the application of this technology, the simplification of the diagnostics and the combination with machine learning algorithms are two important directions for future study.

4.2. The Mechanism of Laser Cleaning

The main mechanisms of laser cleaning were evaporation, spallation, and shockwave generation [5]. As the laser beam irradiated on the surface, the instantaneous temperature was very high, and the contaminant could be ablated by the evaporation effects. The spallation effect mainly resulted from thermal stress at the interface of the contaminated layer and the substrate layer. Additionally, the shock pressure wave induced by the laser inducing a breakdown of gas could cause the removal of contaminants when the fluence of the laser was above the threshold.

According to previous studies, the pulsed laser cleaning mechanism of oxide layers on metals was mainly the spallation effect, although a small part of the oxide layer could also be ablated by the instantaneous high temperature at the top surface of the oxide layer (the evaporation effect) [12,25,26]. At $P_{30\%}$, the intensity of the laser had not achieved the threshold of laser cleaning; the depth of material removal was very small as the melting temperature of oxide was high, and the evaporation effect of nanosecond laser was low. When the laser power was 49 W ($P_{70\%}$), the oxide layer was also ablated by the thermal stress at the interface of the oxide layer and substrate; thus, the removal depth was the same as that at $P_{50\%}$. However, the evaporation effect was improved in this case, and the cleaned surface became brown due to the re-oxidation reaction at elevated temperature.

In addition, the evaporation effect could also induce parallel humps on the cleaned surface, on account of the recoil pressure and surface tensile force in the melting pool [27,28]. At $P_{30\%}$, the inhomogeneous oxide layer was not cleaned, and the surface roughness was increased for the laser scanning. The oxide layer was effectively cleaned at $P_{50\%}$, and the thermal effect was also not very high, so the surface roughness was small. However, the roughness increased to 6.3 μm because the depth of the grooves was increased for the larger laser fluence. Overall, if the optimal parameters of laser cleaning could be obtained by the online monitoring, it could not only reduce the energy cost but also ensure the quality of the cleaned surface.

5. Conclusions

To ablate the oxide layer on the hot-rolled stainless steel, laser cleaning technology coupled with real-time LIBS monitoring was adopted in this study. At varied laser powers, the cleaning process and optical spectra during laser cleaning were investigated. The main conclusions are as follows.

(1) The RIR of the Fe_I-520.9 and Cr_I-589.2 obtained by the monitoring was closely related to the cleaning of the oxide layer on the hot-rolled stainless steel. When the oxide layer was not fully cleaned, the ratio was basically unchanged with increasing laser power because the LIBS signals of the substrate were not excited.

(2) In a practical process, the RIR was suggested to be kept at a relatively small value to avoid over-cleaning. When the RIR sharply decreased at a local region of the surface

to be cleaned, the power of the laser should be increased to ensure the oxide layer was effectively removed.

(3) The surface quality of the laser cleaning was closely related to the laser power. The cleaned surface was bright, and the surface roughness was small when the oxide layer was effectively cleaned. Over-cleaning at a too large laser power resulted in the cleaned surface becoming rough and brown.

Abbreviations

Argon (Ar); Laser-induced breakdown spectroscopy (LIBS); Laser scanning confocal microscope (LSCM); Optical micrograph (OM) Relative intensity ratio (RIR); X-ray diffractometer (XRD); 20% to 90% of maximum power ($P_{20\%}$–$P_{90\%}$).

References

1. Davison, R.M.; Laurin, T.R.; Redmond, J.D.; Watanabe, H.; Semchyshen, M. A review of worldwide developments in stainless steels. *Mater. Des.* **1986**, *7*, 111–119. [CrossRef]
2. Cheng, X.W.; Jiang, Z.Y.; Wei, D.B.; Hao, L.; Zhao, J.W.; Jiang, L.Z. Oxide scale characterization of ferritic stainless steel and its deformation and friction in hot rolling. *Tribol. Int.* **2015**, *84*, 61–70. [CrossRef]
3. Shi, P.Y.; Shi, H.N.; Liu, C.J.; Jiang, M.F. Effect of pickling process on removal of oxide layer on the surface of ferritic stainless steel. *Can. Metall. Quart.* **2017**, *57*, 1–8.
4. Li, L.F.; Caenen, P.; Jiang, M.F. Electrolytic pickling of the oxide layer on hot-rolled 304 stainless steel in sodium sulphate. *Corr. Sci.* **2008**, *50*, 2824–2830. [CrossRef]
5. Marimuthu, S.; Sezer, H.K.; Kamara, A.M. Applications of laser cleaning process in high value manufacturing industries. In *Developments in Surface Contamination and Cleaning: Application of Cleaning Techniques*; Kohli, R., Mittal, K.L., Eds.; Elsevier: Amsterdam, The Netherlands, 2019; Volume 11, pp. 251–288. [CrossRef]
6. Mateo, M.P.; Nicolas, G.; Piñon, V.; Ramil, A.; Yañez, A. Laser cleaning, an alternative method for removing oil-spill fuel residues. *Appl. Surf. Sci.* **2005**, *247*, 333–339. [CrossRef]
7. Veiko, V.; Samohvalov, A.; Ageev, E. Laser cleaning of engraved rolls coupled with spectroscopic control. *Opt. Laser Technol.* **2013**, *54*, 170–175. [CrossRef]
8. Hu, G.Q.; Song, Y.; Guan, Y.C. Tailoring metallic surface properties induced by laser surface processing for industrial applications. *Nanotech. Precis. Eng.* **2019**, *2*, 29–34. [CrossRef]
9. Zhang, Z.Y.; Zhang, J.Y.; Wang, Y.B.; Zhao, S.S.; Lin, X.C.; Li, X.Y. Removal of paint layer by layer using a 20 kHz 140 ns quasi-continuous wave laser. *Optics* **2018**, *174*, 46–55. [CrossRef]
10. Han, J.H.; Cui, X.D.; Wang, S.; Feng, G.Y.; Deng, G.L.; Hu, R.F. Laser effects based optimal laser parameter identifications for paint removal from metal substrate at 1064nm: A multi-pulse model. *J. Mod. Optic.* **2017**, *64*, 1–13. [CrossRef]
11. Zhou, C.; Li, H.G.; Chen, G.Y.; Wang, G.; Shan, Z.Z. Effect of single pulsed picosecond and 100 nanosecond laser cleaning on surface morphology and welding quality of aluminium alloy. *Opt. Laser Technol.* **2020**, *127*, 1061197. [CrossRef]
12. Zhang, G.X.; Hua, X.M.; Huang, Y.; Zhang, Y.L.; Li, F.; Shen, C.; Cheng, J. Investigation on mechanism of oxide removal and plasma behavior during laser cleaning on aluminum alloy. *Appl. Surf. Sci.* **2020**, *506*, 144666. [CrossRef]
13. Li, H.; Costil, S.; Liao, H.L.; Coddet, C. Surface preparation by using laser cleaning in thermal spray. *J. Laser Appl.* **2008**, *20*, 12–21. [CrossRef]
14. Zhang, F.D.; Liu, H.; Suebka, C.; Liu, Y.X.; Liu, Z.; Guo, W.; Chneg, Y.M.; Zhang, S.L.; Li, L. Corrosion behaviour of laser-cleaned AA7024 aluminium alloy. *Appl. Surf. Sci.* **2018**, *435*, 452–461. [CrossRef]

15. Papanikolaou, A.; Jtserevelakis, G.; Melessanaki, K.; Fotakis, C.; Zacharaks, G.; Pouli, P. Development of a hybrid photoacoustic and optical monitoring system for the study of laser ablation processes upon the removal of encrustation from stonework. *Opto-Electro. Adv.* **2020**, *3*, 190037. [CrossRef]

16. Tserevelakis, G.J.; Santiago, P.A.J.; Panagiotis, S.; Siozos, P.; Rivas, T.; Pouli, P.; Zacharakis, G. On-line photoacoustic monitoring of laser cleaning on stone: Evaluation of cleaning effectiveness and detection of potential damage to the substrate. *J. Cult. Herit.* **2018**, *35*, 108–115. [CrossRef]

17. Xie, X.Z.; Huang, Q.P.; Long, J.Y.; Ren, Q.L.; Hu, W.; Liu, S. A new monitoring method for metal rust removal states in pulsed laser derusting via acoustic emission techniques. *J. Mater. Process. Technol.* **2019**, *275*, 116321. [CrossRef]

18. Senesi, G.S.; Carrara, I.; Nicolodelli, G.; Milori, D.M.B.P.; Pascale, O.D. Laser cleaning and laser-induced breakdown spectroscopy applied in removing and characterizing black crusts from limestones of Castello Svevo, Bari, Italy: A case study. *Microchem. J.* **2016**, *124*, 296–305. [CrossRef]

19. Marimuthu, S.; Kamara, A.M.; Whitehead, D.; Mativenga, P.; Li, L.; Yang, S.; Cooke, K. Laser stripping of TiAlN coating to facilitate reuse of cutting tools. *J. Eng. Manuf.* **2008**, *225*, 1851–1862. [CrossRef]

20. Fortes, F.J.; Cabalín, L.M.; Laserna, J.J. The potential of laser-induced breakdown spectrometry for real time monitoring the laser cleaning of archaeometallurgical objects. *Spectrochim. Acta B.* **2008**, *63*, 1191–1197. [CrossRef]

21. Zhang, Y.X.; You, D.Y.; Gao, X.D.; Katayama, S.J. Online Monitoring of Welding Status Based on a DBN Model During Laser Welding. *Eng. J.* **2019**, *5*, 671–678. [CrossRef]

22. Song, Y.; Hu, G.Q.; Zhang, Z.; Guan, Y.C. Real-time spectral response guided smart femtosecond laser bone drilling. *Opt. Laser Eng.* **2020**, *128*, 106017. [CrossRef]

23. Wei, L.L.; Zheng, J.H.; Chen, L.Q.; Misra, R.D.K. High temperature oxidation behavior of ferritic stainless steel containing W and Ce. *Corr. Sci.* **2018**, *142*, 79–92. [CrossRef]

24. Wei, L.L.; Chen, L.Q.; Liu, H.L.; Han, L.Q.; Gong, N.; Misra, R.D.K. Precipitation behavior of Laves phase in the vicinity of oxide film of ferritic stainless steel: Selective oxidation-induced precipitation. *Oxid. Met.* **2020**, *93*, 195–213. [CrossRef]

25. Psyllaki, P.; Oltra, R. Preliminary study on the laser cleaning of stainless steels after high temperature oxidation. *Mater. Sci. Eng. A.* **2009**, *282*, 145–152. [CrossRef]

26. Guo, H.; Martukanitz, R.; Debroy, T. Laser assisted cleaning of oxide films on SUS409 stainless steel. *J. Laser Appl.* **2004**, *16*, 236–244. [CrossRef]

27. Li, N.; Li, Z.; Kang, M.; Zhang, J.M. Numerical simulation and experimental study on laser micromachining of 304L stainless steel in ambient air. *Int. J. Heat Mass Tran.* **2019**, *140*, 978–991. [CrossRef]

28. Li, K.; Zhao, Z.Y.; Zhou, H.M.; Zhou, H.; Jin, J.C. Numerical analyses of molten pool evolution in laser polishing Ti6Al4V. *J. Manuf. Proc.* **2020**, *58*, 574–584. [CrossRef]